

This is a copy of the published version, or version of record, available on the publisher's website. This version does not track changes, errata, or withdrawals on the publisher's site.

Complex dynamics in low electron density lithium ammonia solutions. Interacting modes revealed by comparing neutron and x-ray inelastic scattering

Francesco Sacchetti, Franz Demmel, Eleonora Guarini, and
Caterina Petrillo

Published version information





Citation: F Sacchetti et al. Complex dynamics in low electron density lithium ammonia solutions. Interacting modes revealed by comparing neutron and x-ray inelastic scattering. Phys Rev Materials 6, no. 11 (2022): 115001.

DOI: [10.1103/PhysRevMaterials.6.115001](https://doi.org/10.1103/PhysRevMaterials.6.115001)

This version is made available in accordance with publisher policies. Please cite only the published version using the reference above. This is the citation assigned by the publisher at the time of issuing the APV. Please check the publisher's website for any updates.

This item was retrieved from **ePubs**, the Open Access archive of the Science and Technology Facilities Council, UK. Please contact epublications@stfc.ac.uk or go to <http://epubs.stfc.ac.uk/> for further information and policies.

Complex dynamics in low electron density lithium ammonia solutions. Interacting modes revealed by comparing neutron and x-ray inelastic scattering

Francesco Sacchetti ^{1,2} Franz Demmel ³ Eleonora Guarini ^{4,*} and Caterina Petrillo ¹

¹*Dipartimento di Fisica e Geologia, Università di Perugia, Via A. Pascoli, I-06123 Perugia, Italy*

²*IOM-CNR, c/o Dipartimento di Fisica e Geologia, Università di Perugia, Via A. Pascoli, I-06123 Perugia, Italy*

³*ISIS Neutron and Muon Source, Rutherford Appleton Laboratory, Chilton, Didcot, OX11 0QX, United Kingdom*

⁴*Dipartimento di Fisica e Astronomia, Università degli Studi di Firenze, via G. Sansone 1, I-50019 Sesto Fiorentino, Italy*



(Received 23 June 2022; accepted 25 October 2022; published 8 November 2022)

We present an experimental study of the collective dynamics of lithium-ammonia solutions in order to investigate the role played by the metallic character of the liquid on the atomic dynamics and the relevance of almost free ammonia. To understand the intrinsically complex dynamical behavior due to the presence of clusters composed of at least four ammonia molecules coordinated by a Li atom, we measured the neutron dynamic structure factor in an extended region of wave-vector transfer Q , i.e., from a value as low as 0.2 \AA^{-1} up to 2.4 \AA^{-1} , going beyond the limit of twice the Fermi wave vector $2k_F \simeq 0.98 \text{ \AA}^{-1}$. This allowed us to probe the system with wavelengths between $\approx 3 \text{ \AA}$ (comparable with the ammonia size) and $\approx 30 \text{ \AA}$, a range ensuring a good sensitivity to the collective atomic motions, where the metallic character is known to play a major role. Three different Li concentrations (0.10, 0.17, and 0.20 molar fraction) have been analyzed at 220 K and, in the case of the intermediate concentration, the behavior at 155 K (still in the liquid phase) has also been explored. The effect of the metallic nature, dominated by the electron response when $Q < 2k_F$, is confirmed down to 0.1 molar fraction but, thanks to the availability of better data and the synergy enabled by the simultaneous analysis of neutron and previous x-ray data, we were able to detect the presence of a second excitation affecting the global dynamics of the system. This second mode shows, with respect to the acoustic collective mode, an increasing energy-integrated intensity as Q grows, i.e., in a range where the data obviously better reveal the local (short length scale) atomic behavior. Finally, by comparing the results of the mentioned analysis with those obtained recently by techniques specially focused on the intrinsic metallic properties, like photoemission spectroscopy, it has been possible to correlate the dynamics with the presence of metallic clusters, at almost constant electron density, embedded into free fluid ammonia. The present results also allow for a coherent interpretation of the elastic behavior of lithium ammonia solutions, as determined by ultrasound velocity data in a rather wide concentration range, and the identification of the different concentration regions where agreement with the interacting electron gas paramagnetic response and velocity of collective mode is obtained. Whether the dispersion curve anomaly at $\approx 2k_F$ (observed down to 0.1 molar fraction also for the second mode) is simply related to the dielectric response or some other mechanism may also contribute to this phenomenon, remains an open question.

DOI: [10.1103/PhysRevMaterials.6.115001](https://doi.org/10.1103/PhysRevMaterials.6.115001)

I. INTRODUCTION

Since long time, it is known that liquid metals atomic dynamics shows the presence of long living collective modes in a wide wave-vector range [1–4], with simple metals showing a scalable behavior of the dispersion relation [5]. It is also found that the collective mode velocity can be almost quantitatively accounted for by means of an electron-ion plasma model where the electron screening plays a major role [6–8]. Since the collective dynamics of those metallic systems is strongly related to their electron dielectric response function, the accurate study of the collective excitation acquires a more basic importance to derive useful information on the electron states in liquid metallic systems. For instance, the study of collective

modes allowed to experimentally confirm the negative dispersion of the ion plasma frequency, once the electron plasma is accurately described [8]. However, as the experiments became more accurate, it has been found that the collective modes in liquid metals show additional features depending on specific characteristics of the ion potentials [9–22]. Although all liquid metals show a common behavior in the low momentum region, the very low electron density of lithium ammonia solutions establishes a special case. Accordingly, the behavior of the dielectric function affects the collective motion in a peculiar fashion when $Q \approx 2k_F$ and the resulting anomalous dispersion relation was studied in Refs. [12–16]. In particular, for what concerns the collective modes which are observed at relatively high frequency ($>0.5 \text{ THz}$) using neutron and x-ray inelastic scattering, the indication for the presence of contributions due to atomic dynamics different from the simple propagation of longitudinal acoustic waves is increasing and

*Corresponding author: guarini@fi.infn.it

at least a second mode appears to be important for a precise description of the scattering data. This sort of complexity is not confined to liquid metals as it was observed in molecular liquids like water [23–26] and even in supercritical argon [27].

In metallic systems, starting from the basic model of simple metals where the long wavelength collective dynamics is dominated by the electron screening, one can assume that the only relevant parameter is the electron density, within a uniform electron gas description. This specific view about the longitudinal collective mode dispersion relation is rather well supported by the experiments performed in several metals, where it is possible to scale the dispersion relations as a function of the electron density using a simple extension of the well known Bohm-Staver formula including the ion plasma dynamics [5,8]. Nonetheless, while the THz propagation velocity of the longitudinal acoustic mode is well described by this simple electron gas based model, an increase of the mode velocity is observed as frequency grows from the ultrasound MHz range to the THz region where scattering experiments are performed, though with no evident systematics. In some case, like Hg [7], the collective mode velocity at ≈ 1 THz, c_∞ , is 1.4 times higher than the sound velocity c_0 measured at ≈ 1 MHz. This effect, often referred to as positive dispersion, is even more marked in completely different systems like water [23–26] and many other hydrogen bonded systems [28–38] where a richer dynamics, with more than a single mode, is observed and a ratio $c_\infty/c_0 \simeq 2$ is often found. This behavior was also referred to as *fast sound*, although it is not related to the original definition in the case of binary alloys and mixtures of elements with disparate masses [39,40]. The positive dispersion in lithium ammonia solutions is found smaller than in hydrogen bonded systems, therefore it will be considered as part of the whole dynamics of the system.

Despite the analysis in terms of the electron gas is a good starting point to get a general description of the collective dynamics of liquid simple metals much more has to be done to derive an overall satisfactory account. To this purpose further studies of low electron density systems are important because the electron screening plays a major role when the density is reduced. In particular, lithium-ammonia solutions have an electron density much smaller than the critical density where the compressibility of the interacting electron gas becomes negative, as originally suggested in Ref. [41].

Among low electron density systems, lithium-ammonia solutions are specially interesting because the effective electron gas has a very low density. In the first inelastic scattering experiments on the saturated Li-(NH₃)₄ solution [12–14] an anomalous behavior of the longitudinal collective mode has been observed, namely an evident dip of the dispersion relation at a wave vector close to two times the Fermi momentum $2k_F \simeq 0.98 \text{ \AA}^{-1}$. This fact gave a support to the description of the collective dynamics as driven by the electron density, at least in this momentum range [16]. In parallel, the lithium-ammonia solutions in the metallic phase are found important also because the ion-electron coupling is strong and the large ion size and mass are important in view of the complex arrangement of the ammonia molecules around the lithium ions, which is of interest even in technical applications where the charge redistribution plays a relevant role [42].

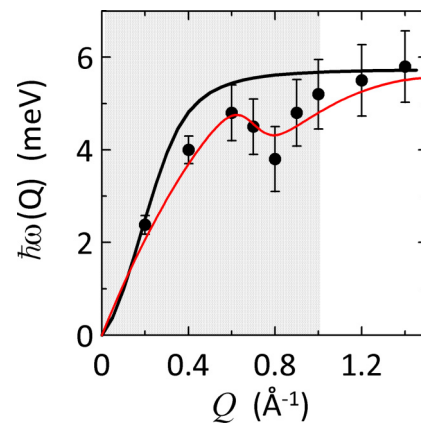


FIG. 1. Dispersion curve of the acoustic longitudinal mode (full line) derived from Eq. (1) for the homogeneous electron gas (see text), compared with the one derived from the INS data at 20 MPM of Ref. [16] (full circles with error bars). The solid red curve is a guide to the eye. The shaded area indicates the region $Q \leq 2k_f$ where it is expected that the electron gas screening plays a significant role.

In recent times, it became possible to perform molecular dynamics simulations based on density functional theory and it was possible to quantify the excess negative charge localized on each ammonia molecule, showing the metallization process. In the case of lithium-ammonia solutions [3,43–45], it was found that an average of about one electron charge is present on the first solvation shell, according to simple evaluations used in previous investigations [16].

To give an account of the effect of the electron gas on the collective dynamics we report in Fig. 1 the simple dispersion relation of the longitudinal acoustic collective mode given by

$$\Omega^2(q) = \Omega_p^2 \left\{ 1 - \frac{1}{\epsilon[q, \Omega(q)]} \right\}, \quad (1)$$

where the electron gas dielectric function, $\epsilon[q, \Omega(q)]$, is calculated self-consistently for the system using an electron gas parameter $r_s = 7.4$ as determined by assuming an electron density equal to the molecular number density of Li-(ND₃)₄ with the ionic mass equal to the molecular one. The above equation is a generalization of the Bohm-Staver approximation and the present calculation is performed along the line employed to study the fast response of an ion plasma coupled with a thermally excited electron gas [46]. Although the bare Coulomb electron-ion potential is employed, the dispersion curve shows a fair agreement with previous neutron scattering results for saturated solutions [16], also shown in the figure, and, as we will show, with the new results of this experiment and data analysis, without the use of any adjustable parameter. This preliminary observation supports the importance of the electron screening present in this exotic metallic system.

Very interestingly, it was recently possible to analyze the electron states in lithium ammonia solutions by means of photoelectron spectroscopy [47], showing that the metallic behavior is governed by the presence of an almost flat electron distribution around the metal ions. Surprisingly, a free electron signature was found even at low MPM (mol % metal, MPM = 100 x , x being the molar fraction of Li) by direct observation of photoelectrons and ab initio molecular dynamics.

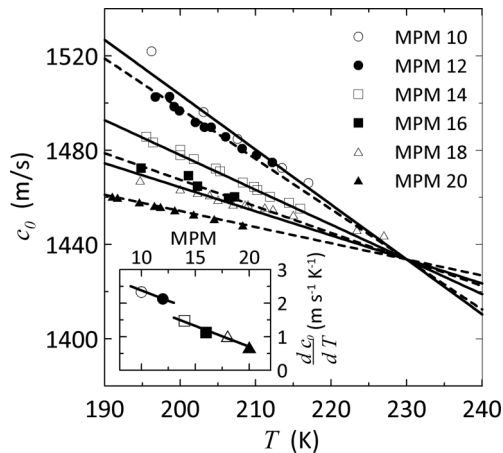


FIG. 2. Sound velocities from Ref. [48] as a function of temperature at different lithium concentrations (symbols for different MPMs are specified in the legend). The straight lines are the linear fits to the data using the model described in the text, from 10% to 20%, and shown alternatively with full lines and dashed lines. (Inset) Slope of the linear fits as a function of concentration (symbols are used according to the legend) and respective linear trends at low and high Li concentrations (full lines).

We also note that the ultrasound velocity as a function of both temperature and solution composition shows a peculiar behavior. In Fig. 2, we report the c_0 velocity data of Ref. [48] as a function of temperature at different compositions. The data are well described by a linear temperature dependence $c_0(T, x) = c_e + \alpha_v(x)(T - T_e)$. By extrapolating the data up to 240 K, we found the indication that at $T_e \simeq 230$ K all the samples in the range 10 to 20 MPM have a similar sound velocity $c_0 = c_e \simeq 1434$ m/s = 9.429 meV Å. This behavior indicates that at $T \simeq 230$ K the sound propagation velocity in the metallic phase is almost independent of the ammonia concentration. Therefore, according to the photoelectron study [47], one can model the system as composed by metallic regions and almost free ammonia in a specific thermodynamic state such that at $T = 230$ K the sound propagation velocity is the same as that of the metallic regions. As the propagation velocity grows faster in pure ammonia than in the metallic regions, on decreasing the temperature the velocity increase is higher as x becomes smaller. The present investigation is devoted to the study of the collective modes of three different lithium ammonia solutions in the metallic liquid phase with MPM = 10, 17, and 20 in a wider momentum region than that explored in previous studies. The measurements were performed at 220 K, where the metallic liquid phase is stable in the whole MPM range and other experimental data are available for comparison purposes in order to obtain a coherent view. The solution with MPM = 17 was also studied at $T = 155$ K, just above the metal to nonmetal transition to look for possible anharmonic effects producing an increase of the collective mode damping, but limiting the study at low Q and in the region close to $2k_F$. The metallic character is shown to be important in the low momentum region where it determines the velocity of the THz collective acoustic mode, while introducing also a paramagnetic behavior of the quite stable metallic clusters around the Li ions, also in agreement with the photoelectron observation [47].

II. EXPERIMENT

According to the above discussion, we performed a new inelastic neutron scattering (INS) experiment in order to extend the measurement of the neutron dynamic structure factor to a larger momentum range at different Li concentrations, looking also for possible temperature effects. We exploited the performance of the high flux three axis spectrometer IN8 installed at the Institut Laue Langevin (Grenoble, France). The experiment was devoted to three different solutions, namely 10 MPM, 17 MPM, and 20 MPM, at a temperature $T = 220.0 \pm 0.5$ K, analyzing also the 17 MPM sample at $T = 155.0 \pm 0.5$ K. The exchanged wave-vector interval ranged from 0.2 \AA^{-1} to 2.4 \AA^{-1} in the energy transfer window from -8 meV to $+8$ meV.

The new neutron data, analyzed together with those of the previous experiment[14], and the inelastic scattering x-ray (IXS) data of Refs. [13,15], provide an extensive description of this metallic system supporting the presence of an additional low-energy mode, not previously observed, interacting with the longitudinal collective oscillations, which are generated by the direct coupling of the ions to the low density electron gas. The advantage of using both INS and IXS data on a complex system lies in the different scattering amplitudes of the various atoms for the two probes. Indeed, neutrons strongly couple with the deuterium atoms and weakly with nitrogen, while x-rays couple strongly with nitrogen atoms and very weakly with hydrogen, while Li atoms produce a very small scattering in both cases.

The possible effects connected to the molecular structure of the lithium ammonia complex are described by adding a second collective mode in the analysis similar to what was found in other metallic [18,21] and non metallic [27,49] liquids and glasses. To distinguish the effect of mode-mode interaction from the electron gas interactions, the experiment was extended at momentum transfers well beyond $2k_F$, i.e., well above the range where the electron gas plays a major role. The different coupling of neutrons and x-rays with the system helps in identifying the characteristics of the two modes.

The measurements were carried out by using a set of tight collimations ($30'$, $20'$, $20'$, $20'$ from reactor to detector) with Cu(200) and Cu(111) as monochromator and analyzer, respectively. The final wave vector of the neutrons was held fixed at $k = 4.1 \text{ \AA}^{-1}$ and the incoming one k_0 was varied to obtain the desired transfer of energy ($\hbar\omega$) and momentum ($\hbar Q$). The elastic energy resolution was determined using a vanadium slab having the same dimensions as the sample obtaining a Gaussian resolution function with a full width at half maximum of 1.07 meV. The samples were produced inside the titanium cell used for the experiment by liquefying a known quantity of anhydrous, 99% deuterated, ammonia onto a pre-weighted quantity of natural Li under He atmosphere [14]. The sample temperature was 220 K held constant within 0.5 K, apart from the smaller set of measurements performed at 155 K. Accurate measurements of background were also performed according to the procedure described in Ref. [14] and the data were reduced by correcting for the background contributions, multiple scattering and sample transmission. The final data were normalized to the vanadium standard in such a way that the energy integral of the dynamic structure

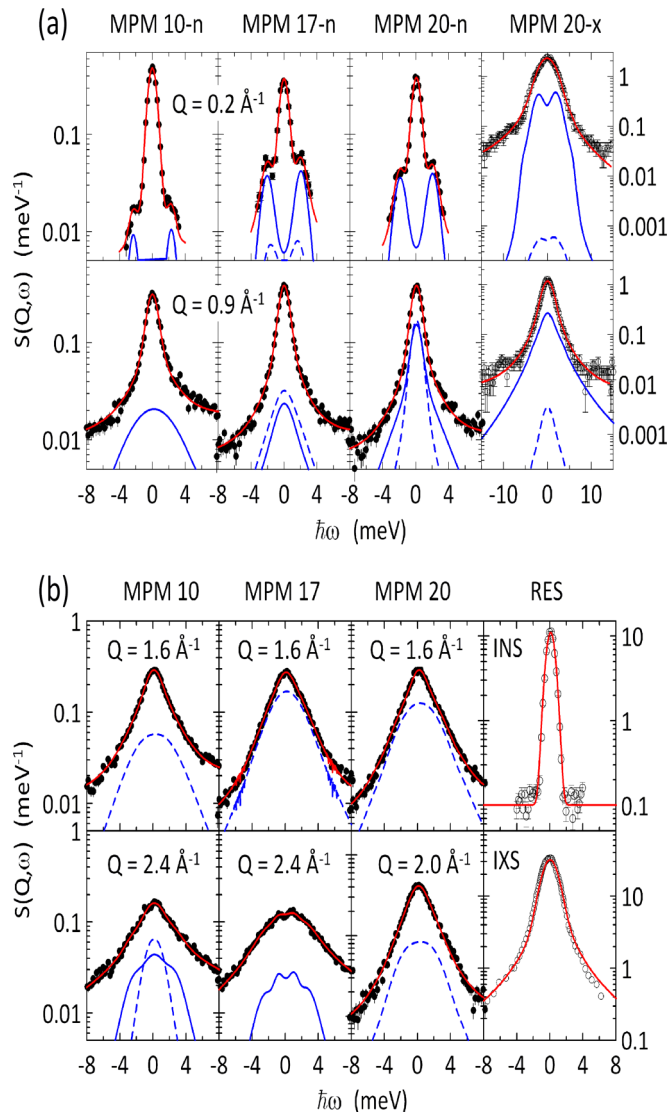


FIG. 3. Experimental results (black dots) compared with the fitting curve (red full lines) according to the model described in Sec. III. (a) Data for the three samples (MPM = 10, 17, and 20) from INS and for the sample MPM = 20 (black circles) in the case of IXS data [13] at selected values of Q [0.2 \AA^{-1} (top) and 0.9 \AA^{-1} (bottom)]. The blue full and dashed lines refer to the two modes $j = 1$ and $j = 2$, respectively, identified as longitudinal and quasi-optic modes. When either the full or the dashed line is absent indicates a negligible contribution from the mode. (b) INS data (black dots) at higher Q values for the same samples. The lines are as in panel (a). Typical resolution functions for INS (right top) and IXS (right bottom) are reported. The red lines are fits to the experimental resolution functions.

factor is equal to the static structure factor $S(Q)$, with the asymptotic condition $S(Q) = 1$ as $Q \rightarrow \infty$.

Typical results from the present INS experiment are reported in Fig. 3 where we see the evident inelastic peaks due to the longitudinal collective mode at $Q = 0.2 \text{ \AA}^{-1}$, evolving on increasing the momentum. Looking at the data a complicate evolution is visible and, in the case of the sample 17 MPM, a low-energy ($< 2 \text{ meV}$) structure is present at $Q = 2.4 \text{ \AA}^{-1}$, a fairly high wave-vector transfer. In Fig. 3, we report also

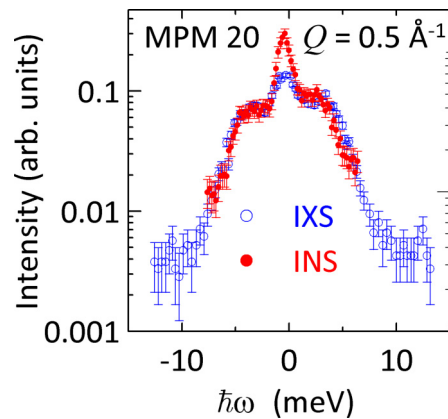


FIG. 4. Experimental results at $Q = 0.5 \text{ \AA}^{-1}$ for the sample MPM = 20 measured by INS (red dots) compared to the sample MPM = 20 measured by IXS [13] (blue circles). The IXS data are scaled to the INS ones in order to have a similar intensity of the inelastic peaks, without further modifications.

a set of x-ray data at 20 MPM from Ref. [13], where it is observed that the inelastic features appear to be similar but less evident due to the specific shape of the instrumental energy resolution function. In the low- Q region, where the most evident inelastic scattering is due to the collective longitudinal mode there are only minor differences between neutron and x-rays as it is seen in Fig. 4 where x-ray data from Ref. [13] at $Q = 0.5 \text{ \AA}^{-1}$ are reported on the same scale of the present neutron data, using as reference values the intensities of the inelastic peaks. Notice the minor effect of the sharper resolution of the INS data at low energy, and the presence of the quasielastic incoherent scattering which makes, expectedly, the central quasielastic peak stronger in INS than in IXS.

III. MODELING THE SCATTERING DATA

According to the most recent findings in several different systems we analyze the lithium ammonia data, using available data from neutron and x-ray scattering, by means of a single model able to describe all of them within a coherent scheme.

In all previous experiments on lithium-ammonia solutions, either with neutrons or with x rays, the models were used to enhance the effect related to the metallic characteristic of the sample as a whole. As noted before, due to the chemical composition of the system, the cross section in the case of INS is mainly due to the deuterium dynamics, while, in the case of IXS, the hydrogen atoms are practically invisible and the dominant part of the signal comes from the nitrogen atoms. Therefore, by comparing neutron and x-ray data with the same model, it is possible to obtain more information on the distribution of the atomic dynamics on the different parts of the lithium-ammonia complex.

In general, since the hydrogen atoms are strongly bound to the nitrogen one can expect that the longitudinal collective mode is similar in neutron and x-ray experiments, as it was actually found. However, small effects could come out due to specific (collective) motions of the hydrogen atoms related to re-arrangements of the ammonia molecules around the Li ion. Looking at the phonon dispersion curves in solid ammonia

[50] one finds several optic modes in the range 10 meV to more than 50 meV. Considering that the ammonia molecules in the lithium solutions could be more loosely bound to each other, optic-like modes are possible at a lower energy and hence they are likely to cross the dispersion relations of the longitudinal acoustic mode.

Therefore the model based on more than one mode, interacting with each other, is employed [4] where the combination of two basic modes, described by the amplitude operator Q_{Qj} , were employed by assuming the same dynamic characteristics, that is energy ($\hbar\omega_{Qj}$) and self-energy $[(\sigma_j(Q, \omega))]$, identified by a branch index $j = 1$ and 2. As in other investigations the self-energy was approximated by its simplest form having the correct ω dependence, that is $\sigma_j(Q, \omega) = i\Gamma_j(Q)\omega$, where $\Gamma_j(Q)$ depends only on Q and, in the low damping limit, is the full width at half maximum of $S_{jj}(Q, \omega)$.

This model [4] is known to be able to provide a straightforward description of the positive dispersion and the global evolution of the measured dynamic structure factors of Fig. 3. This transition cannot be described using a simple electron gas model [14,16] because it is due to an additional interaction

due to the disordered nature of the liquid which introduces a strong damping of all the vibrational dynamics.

Within this model the dynamic structure factor of the sample is given by

$$S(Q, \omega) = S_{qe}(Q, \omega) + [n(\omega) + 1] \sum_{jj'} A_{jj'}(Q) S_{jj'}(Q, \omega), \tag{2}$$

where $n(\omega)$ is the Bose factor, $S_{qe}(Q, \omega)$ is a quasielastic contribution accounting for, both atomic and thermic, diffusionlike effects, and $S_{jj'}(Q, \omega)$ is the dynamic structure factor directly related to the Fourier transform of the time dependent correlation function $\langle Q_{Qj}^\dagger(0) Q_{Qj'}(t) \rangle$, which in turn, can be obtained from the proper equation of motion [51] after establishing the system hamiltonian. Using the equation of motion of the density-density correlation function it can be shown that $S_{jj'}(Q, \omega)$ is given by the imaginary part of the jj' element of the inverse of the matrix $M_{jj'}(Q, \omega) = \{\delta_{jj'}[\omega^2 - \omega_{Qj}^2 - \sigma_j(Q, \omega)] + U_{jj'}(\mathbf{Q})\}$. Here $U_{jj'}(\mathbf{Q})$ is a $j - j'$, Q dependent, coupling function. When only two modes are taken into account, the explicit form for $S_{jj'}(Q, \omega)$ is as follows:

$$S_{jj'}(Q, \omega) = -\frac{1}{\pi} \left\{ \frac{\sum_k [\omega^2 - \omega_{Q,k}^2 - \sigma_k(Q, \omega)] (1 - \delta_{jk}) \delta_{jj'} + U_{jj'}(Q) (1 - \delta_{jj'})}{D(Q, \omega)} \right\}, \tag{3}$$

where $D(Q, \omega)$ is the determinant of $M(Q, \omega)$ and is given by

$$D(Q, \omega) = [\omega^2 - \omega_{Q1}^2 - \sigma_1(Q, \omega)][\omega^2 - \omega_{Q2}^2 - \sigma_2(Q, \omega)] - |U_{12}(Q)|^2. \tag{4}$$

Here we have included the diagonal terms $U_{jj}(Q)$ into ω_{Qj}^2 because they produce just an energy renormalization which cannot be observed.

The application of a model like the present one needs further approximation to avoid an over interpretation of the experimental data. In addition to the use of two modes only, we neglect the contribution of $S_{jj'}(Q, \omega)$ when $j \neq j'$, assuming a negligible mixed structure factor. Following the procedure used in other experiments [24,37], the interaction is approximated using two constants only, that is a strength β_0 times an exponential Q -dependent decay function, namely by $U_{12}(\mathbf{Q}) \simeq Q\beta_0 \exp[-\lambda Q]$, so that the model automatically accounts for the positive dispersion as described below.

The present INS data span a Q range wider than the position of the main diffraction peak of $S(Q)$ [52,53], $Q_0 \simeq 1.9 \text{ \AA}^{-1}$, therefore the approximations $\omega_{Q1} \simeq c_\infty Q$ for the longitudinal acoustic mode, useful when Q is smaller than the size of the pseudo-Brillouin zone $Q_{PBZ} = Q_0/2$, and ω_{Q2} is almost constant, cannot be used in the whole momentum interval we explored. Accordingly, at each Q value, we need a model with a total of ten free parameters: four dynamic parameters for the positions and damping constants of the two modes, two other parameters for the amplitude and width of the quasielastic peak described by a Lorentzian function, and two parameters describing the amplitudes of the two inelastic modes. The last two parameters are the strength of the interaction β_0 and its Q decay constant λ , which is expected to depend on the temperature and sample composition. The dynamic parameters are assumed to be the same for both

INS and IXS, while all four amplitudes are different for the two probes together with the widths of the quasielastic peaks. This last choice was dictated by the fact that the quasielastic peak is not due to the collective motion but it combines different processes mixing in a different way for the two probes.

The model has indeed many free parameters. However, thanks to the different visibility of hydrogen/deuterium, different shape of the resolution function and other differences in INS and IXS experiments, the use of a single dynamic model for both cases strongly supports the validity of the overall results we obtained in the common INS-IXS momentum range. In particular, we first considered the momentum range and compositions where both INS and IXS data are available. In this case, the fit of both INS and IXS data was performed using the *same* dispersion relation and damping. Therefore this procedure was applied to samples having 16 MPM for IXS and 17 MPM for INS, assumed to be equivalent, and 20 MPM, limiting the analysis to $Q \leq 1 \text{ \AA}^{-1} \simeq Q_{PBZ}$. This fit was found to produce well defined results which were then used as starting point to apply the procedure to the other INS data. We found a satisfactory fit in all cases and, the need of an additional mode was rather evident, as seen in Fig. 3 for the INS high Q data.

After the fit to the INS and IXS data, smoothed dispersion relations and damping functions were produced to perform a fit of all the data with a fixed dynamic model. Typical results for the final fitted dynamic structure factor $S(Q, \omega)$ are reported in Fig. 3, together with the two components

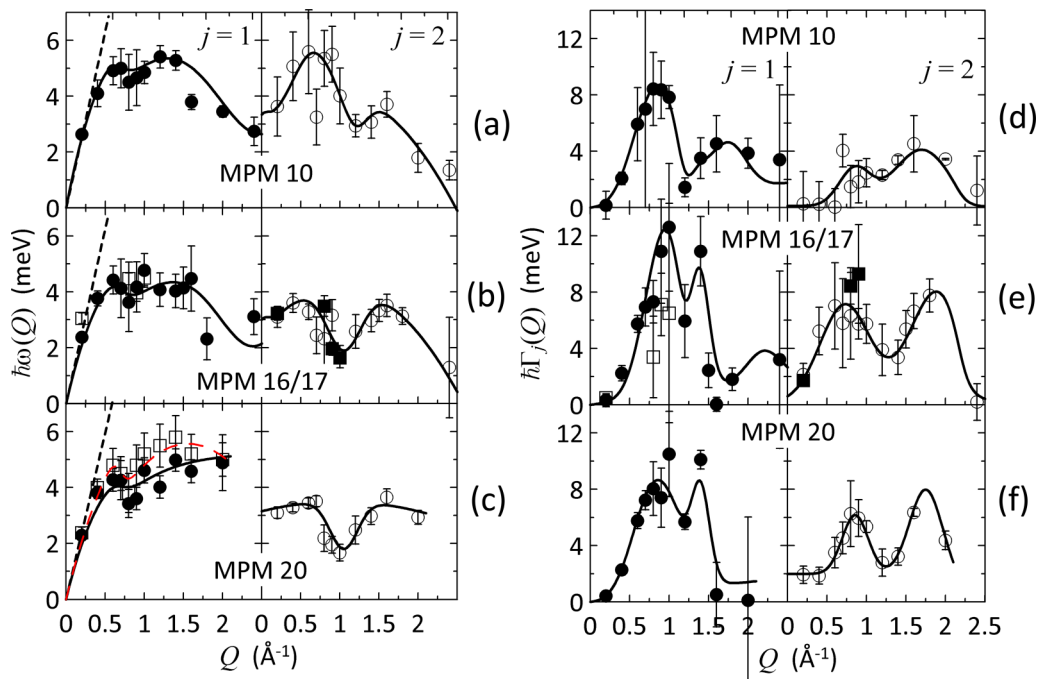


FIG. 5. Dispersion curves of the bare energy $\hbar\omega_{Qj}$ [(a)–(c)] and damping $\hbar\Gamma_j(Q)$ [(d)–(f)] as derived from the present INS and IXS data, which have been fitted together to produce a common dispersion relation. These data refer to the MPM 16/17 and 20 samples. In the case of the 10 MPM sample, only INS data could be used. The black dots are used for mode $j = 1$, while the empty circles for mode $j = 2$. The open squares and the full squares at 16/17 MPM refer to the present low temperature INS data. The full lines represent the smoothed dispersion relations used for the final global analysis of all the scattering data. The straight black dashed lines through the origin in the dispersion curves correspond to the linear behavior $c_\infty Q$. The open squares at 20 MPM for the $j = 1$ mode are the result of a single DHO fit to the previous INS data of Ref. [16] and the red long dashed curve is a guide to the eye, as already reported in Fig. 1.

$A_{11}(Q)S_{11}(Q, \omega)$ and $A_{22}(Q)S_{22}(Q, \omega)$, in comparison with the experimental data.

Of course, there is no way to classify each mode using only the measurement of $S(Q, \omega)$ because this function is related to the longitudinal density fluctuations, so that only the longitudinal projection of the modes is observed. It is expected that a small mode amplitude indicates the presence of rather intense transverse component, but this remains a qualitative guess which is even less valid in the case of optic-like modes, where the local structure is important in determining the observed intensity.

IV. RESULTS FROM THE MODEL FITTING AND DISCUSSION

To derive the physical information we can first consider the dispersion curves we obtained from the general fit presented in Fig. 5. It is found that the dispersion curves for the samples 20 and 16/17 MPM are very similar with a change of the high frequency, low Q , collective mode velocity from $c_\infty = 11.9 \pm 0.5 \text{ meV \AA} = 1810 \pm 30 \text{ m/s}$ to $c_\infty = 12.5 \pm 0.2 \text{ meV \AA} = 1920 \pm 80 \text{ m/s}$. The evolution of the dispersion curve on increasing Q is similar apart from the fact that the energies at 16/17 MPM are about 5 to 10% higher. From these results it is straightforward to classify mode 1 as a *longitudinal acoustic* mode because its evident linear decrease with $\omega_1(Q) = c_\infty Q$. Moreover, in the region $Q < 0.4 \text{ \AA}^{-1}$, we can safely assume, other than $\omega_1(Q) = c_\infty Q$, $\omega_2(Q) \approx \omega_0$ so

that the $S(Q, \omega)$, in the low damping limit, expected when $Q \rightarrow 0$, will show the presence of two excitations having the following dressed energies [24,25]:

$$\begin{aligned} \omega_1(Q) &= Q \sqrt{c_\infty^2 - \frac{\beta_0^2}{\omega_0^2}} = Q c_0, \\ \omega_2(Q) &= \omega_0, \\ \frac{c_0}{c_\infty} &= \sqrt{1 - \frac{\beta_0^2}{\omega_0^2 c_\infty^2}} < 1. \end{aligned} \quad (5)$$

This last equation was used to determine β_0 using the available c_0 data to interpolate the estimate of c_0 for all samples and temperature. After exploratory tests, the interaction decay parameter was fixed as $\lambda = 1.5 \text{ \AA}$ because the interaction has its effect mainly at $Q \approx 0.4 \text{ \AA}^{-1}$ where the two bare dispersion curves ω_{Q1} and ω_{Q2} cross each other and the decay of the interaction has a minor effect on the global fit.

This model describes correctly the positive dispersion as Q is increased from a very low value to the range explored by the INS and IXS experiments. The results of the interaction at low Q are reported in Table I where both the INS and IXS contribute to define the fitting parameters for the common data. Velocity data from ultrasound experiments [48] are also reported together with the ratio c_∞/c_0 .

Looking at the dispersion relations (Fig. 5), we note that $\omega_1(Q)$ shows a mild dip when $Q \approx 0.8 \text{ \AA}^{-1}$, a value

TABLE I. Interaction strength β_0 , velocity of longitudinal collective mode c_∞ at $Q \rightarrow 0$ and $\hbar\omega_0$. The low Q velocity c_0 derived by interpolation from the ultrasound measurements [48] and ratio c_∞/c_0 are also reported. All the data are presented as a function of the MPM and temperature, where we indicated the “equivalent” data sets for neutrons and x rays (neutrons/x rays). IXS data considered in the present analysis are those of Refs. [13,15]. NA stands for “Not Available.”

T (K)	MPM	$\hbar^2\beta_0$ (meV ² Å)	$\hbar c_\infty$ (meV Å)	$\hbar\omega_0$ (meV)	$\hbar c_0$ (meV Å)	c_∞/c_0
220/NA	10	30.0 ± 2.0	13.9 ± 0.4	3.0 ± 0.1	9.66 ± 0.05	1.44 ± 0.07
220/240	17/16	23.0 ± 1.2	12.5 ± 0.2	2.8 ± 0.1	9.43 ± 0.05	1.32 ± 0.04
155/NA	17	$36. \pm 5.$	15.3 ± 1.2	3.1 ± 0.2	9.96 ± 0.05	1.54 ± 0.12
220/240	20/20	23.2 ± 2.7	11.9 ± 0.5	3.2 ± 0.1	9.43 ± 0.05	1.26 ± 0.09
255/NA	20	23.2 ± 2.7	11.8 ± 0.5	3.2 ± 0.1	9.32 ± 0.05	1.27 ± 0.09

comparable with $2k_F \simeq 0.98 \text{ \AA}^{-1}$, as observed since the first investigation [12] and in subsequent studies [13–15], where a single damped harmonic oscillator was used to analyze the data. This dip indicates the presence of a decay channel of the longitudinal acoustic mode through a rather strong electron-phonon interaction one could attribute to the very low electron density. However, the present more accurate data indicate the presence of the second mode $\omega_2(Q)$ having a much more visible dip in the same Q region, although shifted at a slightly higher Q , even closer to $2k_F$ than in the longitudinal case. Actually, the second mode is expected to originate from the ammonia clusters around the Li atoms mechanisms, other than the simple electronic screening, may account for the shape of its dispersion and damping Q dependence. However, it might well also be that the dip in the two cases has exactly the same explanation, but is more precisely located in Q when it leaves a more marked fingerprint (mode 2). For comparison purposes, we report in Fig. 1 the present smoothed dispersion relations for the 20 MPM sample together with the homogeneous electron gas calculation according to Eq. (1). It is seen that the calculation accounts correctly for the velocity of the longitudinal mode at low Q but, as already observed, it does not show a dip when approaching $2k_F$ because the calculation accounts for the electron-electron interactions only, and the dielectric function does not show any particular trend. Moreover, the formulation is appropriate only at low Q because the momentum dependence of the plasma frequency Ω_p is not included and the electron-ion interaction is assumed to be that of a pointlike particle.

Considering the overall behavior of the dispersion relations shown in Fig. 5, we conclude that at $Q < k_F$ and THz frequencies the system behaves like a uniform material at all explored MPM values. In other words, the addition of ammonia to the saturated solution has a limited effect, and the metallic regions seem to govern the propagation of the density fluctuations. The presence of ammonia seems to contribute with an additional mode at lower energy which slightly modifies the $j = 1$ mode dispersion relation.

From the present data, from those of Ref. [48] about the density and the sound velocity, and from those of the recent photoemission experiment [47], in addition to the results of computer simulations [43–45], the presence of metallic regions having fixed dynamic and electronic properties is strongly supported.

One can also observe that in the region $Q \approx 2k_F$ the stronger effect visible in the dispersion curve of the lower

energy mode $\hbar\omega_2(Q)$ is also present in its intensity. To evaluate the strength of each mode, we can consider the static structure factor $S(Q)$, which is equal to the frequency integral of $S(Q, \omega)$. This quantity is composed of three components, namely $S_{qe}(Q)$ due to the quasielastic contribution, $S_{11}(Q)$, due to the mode $j = 1$, and $S_{22}(Q)$, due to the mode $j = 2$. These contributions are different for INS and IXS as a consequence of the different coupling with different atoms of the two probes. The INS data for $S_{11}(Q)$ and $S_{22}(Q)$ are reported in Fig. 6 where it is seen that the $j = 2$ mode has a peak located at about 1 \AA^{-1} , a momentum similar to $2k_F$, while at 10 MPM the peak is reduced. Although the intensity is related to different factors this result supports the existence of the metallic regions with fixed properties. It is interesting to observe that a peak is present in the same region, $Q \approx 2k_F$, also in the damping $\Gamma_j(Q)$ of both modes. In the previous investigation [16], the model based on a single damped harmonic oscillator produced a continuous increase of the damping with a constant slope and a small jump at $Q \approx 0.9 \text{ \AA}^{-1}$. The present, more accurate investigation, based also on the combination of INS and IXS data, provides a complex picture where it is again shown that the region $Q \approx 2k_F \simeq 0.98 \text{ \AA}^{-1}$ is important and probably related to a strong electron-phonon interaction.

Looking at the fractional intensity of the modes, one can also observe that mode $j = 1$ contributes in a similar way to both INS and IXS while the mode $j = 2$ gives a minor contribution in the IXS case, so that one can conclude that this mode is mainly due to the hydrogen (deuterium for INS) atoms, at least in the $Q < 1 \text{ \AA}^{-1}$ region where the IXS data are available.

On the contrary, $S_{qe}(Q)/S(Q)$ from INS and IXS is similar when $Q < 0.8 \text{ \AA}^{-1}$, while the IXS one becomes greater on increasing Q , therefore the slow dynamics of the system is expected to be related to the nitrogen atoms, while the slow dynamics on the hydrogen atoms seems to be concentrated on a low-energy collective motion which has a rather strong damping but it is not overdamped [$2\omega_2(Q) > \Gamma_2(Q)$] in the whole range we explored.

To investigate the role of the interstitial ammonia we observe that the density [48] of the solutions can be accurately described in the range $10 < \text{MPM} < 20$ and $190 \text{ K} < T < 230 \text{ K}$ as a mixture of metallic fraction having a density equal to that of the 20 MPM solution and interstitial ammonia having the density equal to that of pure liquid ammonia along the coexistence curve [54]. At the same time the sound velocity c_0 is described by a linear trend as shown in Fig. 2. The

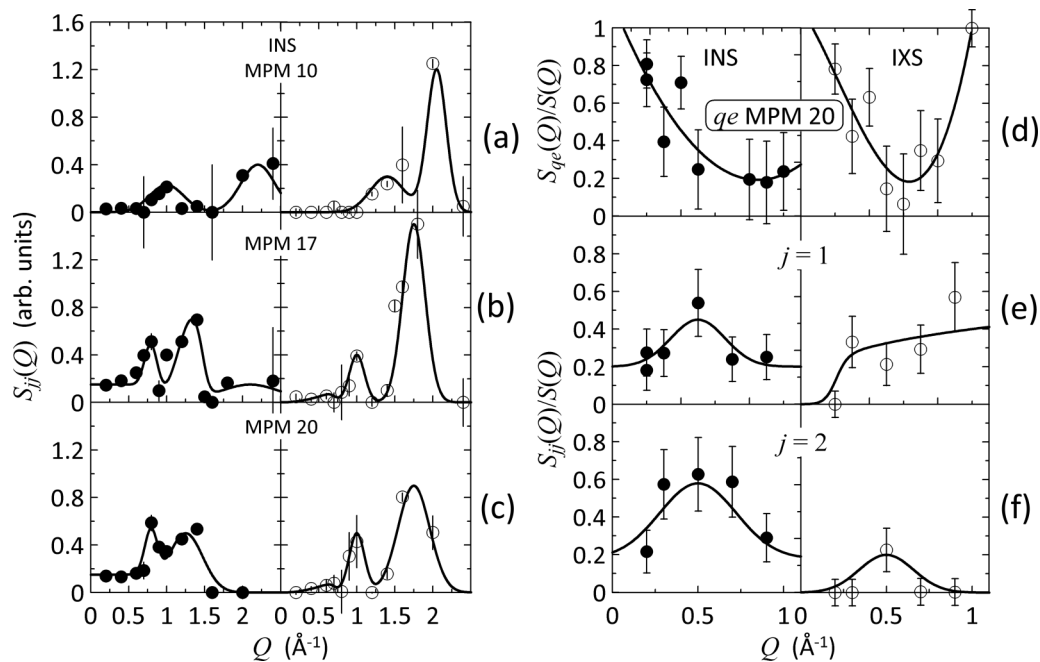


FIG. 6. [(a)–(c)] Integrated intensities, $S_{11}(Q)$ and $S_{22}(Q)$, of the two modes as a function of wave-vector transfer, normalized to the static structure factor $S(Q)$, for the three samples as deduced from INS at $T = 220$ K. Full dots are used for the $j = 1$ mode, while empty circles for the $j = 2$ one. The full lines are guides to the eye. (d) Intensity ratio $S_{qe}(Q)/S(Q)$ for INS (left side) and for IXS (right side) for the 20 MPM concentration. (e) ($j = 1$) and (f) ($j = 2$): intensity ratios $S_{jj}(Q)/S(Q)$ in the case of INS (left side) and IXS (right side) at 20 MPM and 220 K.

interesting quantity is the slope dc_0/dT reported in the inset of Fig. 2 where it is seen that two different regions exist. One finds that dc_0/dT is increasing on decreasing the MPM but a jump is present at $\text{MPM} \approx 13$. This behavior appears to be correlated to the increase of the interaction parameter in the THz range (see Table I) where an increase of β_0 is seen in going from 20 to 10 MPM, though the limited number of compositions investigated in the scattering experiments does not allow for a more precise correlation. Considering that the photoelectron experiment [47] indicates that the metallic complexes maintain their electronic characteristics on decreasing MPM, the observed changes are to be connected with the state of the interstitial ammonia.

The present investigation was extended to the higher Q region, in addition to the low momentum region where the system is dominated by its metallic character. In the case of the two samples with MPM equal to 10 and 17, INS data up to $Q = 2.4 \text{ \AA}^{-1}$ have been collected. As shown in Fig. 3 a different behavior as a function of the Li fraction is obtained at the highest Q . At 17 MPM $S(Q, \omega)$ shows a peak at about 1 meV. The overall shape of the $S(Q, \omega)$ suggests also the presence of another broader excitation at about 3 meV. Therefore the two mode description was employed also at high Q values. The 10 MPM sample shows a less structured $S(Q, \omega)$ but the same model provides a good description also in this case.

Further information is available from the damping factors $\Gamma_j(Q)$ of the two modes, as reported in Fig. 5. We see that both $\Gamma_1(Q)$ and $\Gamma_2(Q)$ have a broad peak when $Q \sim 0.8 \text{ \AA}^{-1}$ in all systems with some change in the case of the $j = 2$ mode. This peak could be related to the behavior of the dispersion relation

at $Q \simeq 2k_F$ as previously observed [12,14]. This behavior was already attributed to the presence of a strong decay channel due to the electron-phonon interaction, which weakens at low MPM where the electron distribution becomes less uniform and the total number of electrons is reduced, but it is still present.

However, in this investigation the low Q trend shows a different behavior probably composed by a lower momentum part where the trend is closer to a quadratic one, as expected in the hydrodynamic limit, and a higher momentum part where a linear trend develops. It is also interesting to note that, in all cases, a decrease of $\Gamma_1(Q)$ is seen when Q approaches Q_0 . However this result has a limited validity because the mode is rather weak.

According to these data it is reasonable to assume that the dispersion relations of the two modes at high Q are the prolongation, shown in Fig. 5, of those observed at low Q . The prolongation of the longitudinal acoustic mode shows an energy decrease in crossing $Q_0 \simeq 1.90 \text{ \AA}^{-1}$. This behavior is similar to that of a crystalline system when the momentum transfer is close to a reciprocal lattice point. The energy decrease is not present at 20 MPM where the mode $j = 1$ becomes weaker and the determination of $\omega_1(Q)$ is less accurate.

From the previous investigations of the collective modes in lithium ammonia solutions there is no information about the temperature dependence of the THz dynamics. In the case of the 17 MPM sample, we investigated the Q region below $2k_F$ also at 155 K and we found some temperature dependence of the collective mode velocity, while the behavior close to $2k_F$ does not display visible changes. However the increase of both c_0 and c_∞ is evident in Table I. In particular, c_∞/c_0 increases

of about two standard deviations, a growth connected to the increase of the interaction parameter β_0 . The limited set of data indicates that this result needs a specific investigation but we can state that a temperature reduction of 30% does not affect the general trend of the collective modes apart from the increase of β_0 affecting the positive dispersion. This behavior supports the observation that the damping factor mainly originates from disorder and electronic interaction and no relevant anharmonic effects are present as seen for instance in liquid gallium [11] at a much higher temperature.

As to the mode integrated intensities, reported in Fig. 6, an intensity decrease of the $j = 2$ mode at 10 MPM can be seen at Q values below $2k_F$, indicating that the electron-mediated interaction is still active. In the same Q range, for the high Li concentration samples (17 and 20 MPM), an increase of the intensity of the $j = 2$ mode, quite well localized in a narrow momentum interval, is observed. This increase apparently compensates the tendency to a loss of intensity of the longitudinal acoustic mode. Such an effect could, once again, be attributed to the electron-mediated interaction which produces an energy decrease of both modes, but in such a way that the mode-mode interaction tends to transfer oscillator strength from the longitudinal acoustic mode to the second one. The presence of this strong interaction can likely be a consequence of the low Fermi energy $E_F = (\hbar k_F)^2/2m \simeq (1.9192/r_s)^2 \text{au} \simeq 915 \text{ meV}$ of the present low density electron gas, where the dielectric function was shown to become negative [16]. Although the Fermi energy is rather low, it corresponds to a temperature $T_F \simeq 10620 \text{ K}$, which is much higher than the temperature of all the experiments in the metallic liquid phase. Accordingly, all the estimates obtained from the electron gas can be safely produced using zero temperature approximations. Of course, the electron gas driven long range interactions play a major role in the low momentum region, while the ammonia clusters play a role on the local properties like the $j = 2$ mode.

V. CONCEPTUAL SYNOPSIS AND FINAL COMPARISON WITH MAGNETIC SUSCEPTIBILITY RESULTS

This experiment and data analysis which includes also available x-ray data, provide conclusions about the THz density fluctuations in lithium-ammonia solutions, where the low electron density metallic character produces unusual effects on the ion dynamics, a property which can be important in many other complex systems where similar electron distributions are present. To extend the knowledge on this system the experiment and the analysis covered a wider Q range than that up to $2k_F$, going beyond the region where the role of the electron interactions are very important.

The existence of metallic clusters with almost fixed electron density in a wide range of total metal concentration is now enhanced by the photoelectron observation [47]. This observation supports the model where well defined $\text{Li}-(\text{NH}_3)_4$ metallic clusters are embedded into an *almost free ammonia* matrix so that some metal fingerprints are present down to low MPM values. The low electron density ($r_s \simeq 7.4$) of the metallic clusters, well below the electron gas critical value, plays a very important role for basic science and applications of these materials, therefore the present results, together with

other information, are important to define the correct modeling of these and other systems where the valence electrons have similar distributions.

The proposed model where the metallic complex is weakly dependent on the MPM is supported by all the available data. The density of the solutions is consistent with a slow evolution of the density of the free ammonia and almost constant density of the metallic complexes, as suggested by the photoemission data in a wide concentration range. The presence of this complex dynamics where small metallic clusters play a basic role can be related also to the recent observation of evident anomalies of the collective modes in liquid rubidium [55]. The presence of small metallic clusters could be a common feature of the low density electron gas where only a *negative* pressure can stabilize the system [41].

Further information on the electronic state could be derived from the plasmon dispersion relation observed in the range 8–20 MPM [56]. However this information seems difficult to interpret because there is a technical limit in subtracting the contribution of the huge quasielastic scattering which includes both elastic and ion-dynamics scattering. The comparison with the simple random phase approximation (RPA) looks quite inappropriate at low density. In particular, on reducing the electron density, the plasmon dispersion coefficient is known to decrease well below the RPA value and to become even negative [57] when r_s is higher than about 5. Nonetheless, also a qualitative analysis of the data shows that the plasmon damping increases on decreasing the MPM, while the plasmon energy does not show a large change. Qualitatively, again, the interpretation could be based on the assumption that the metallic complexes are embedded in the liquid ammonia. The small size of the metallic islands can be the origin of the increasing plasmon damping on reducing the lithium content. Further investigation of the plasmon behavior would be necessary to complement the other observations.

Another useful information on electron states comes also from the measurement of the magnetic susceptibility. Although the available data [58] do not provide accurate enough data there is an indication that a paramagnetic trend is present in a wide MPM range, down to small values. Unfortunately, the paramagnetic contribution is fairly small because the Pauli susceptibility decreases on increasing r_s and the ammonia molecules contribute with their diamagnetic response within this environment [58]. However, using the simple picture we discussed so far, one can assume that at fixed temperature the ammonia has a fixed diamagnetic susceptibility χ_a .

Using the measured susceptibility of free ammonia at $T = 233 \text{ K}$ as determined in the 0 MPM limit one can assume $\chi_a = -8.89 \times 10^{-6}$ (SI convention). Assuming that ammonia contributes with this value to all solutions, we find that the Li contribution is almost always positive, as shown in Fig. 7. Apart from the paramagnetic behavior introduced by Li, we can identify, according also to the original experiment [58], three different regimes. When the MPM ranges from 0 to 5 there is a very weak paramagnetic behavior. In the MPM range above 5 the paramagnetic susceptibility increases, while above 10 MPM a sort of plateau appears. This *magnetic transition* appears in a region where less than half of the ammonia molecules are outside the magnetic clusters, probably causing

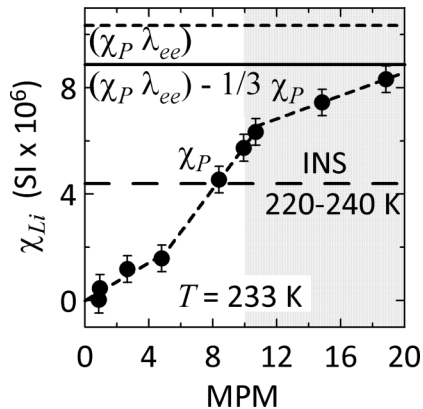


FIG. 7. Experimental magnetic susceptibility from Ref. [58] (full circles) compared with simple estimates based on the homogeneous electron gas at $r_s = 7.4$ and zero temperature. The experimental temperatures displayed in the plot, i.e., either 233 or 220–240 K, are not very low but they are low enough to justify the zero temperature approximation for the electron gas estimates, since the Fermi energy corresponds to a much higher value (see text). The experimental data have been corrected for the diamagnetic contribution of ammonia and reported in SI units. The dashed line through the data points is a guide to the eye. The horizontal lines are as follows: short dashed line paramagnetic electron gas susceptibility including the effect of the electron-electron interaction according to Ref. [59], continuous line paramagnetic susceptibility corrected for the diamagnetic electron gas contribution, long dashed line Pauli susceptibility. The shaded area indicates the MPM region where inelastic scattering data on the atomic dynamics are available.

a minor disturbance of the metallic structures, but still producing an effect on the sound propagation velocity c_0 , as seen in Fig. 2.

Assuming that the plateau is due to an almost uniform electron gas one can try to compare the paramagnetic susceptibility to a theoretical estimate. The simplest estimate comes from the Pauli susceptibility calculated using $r_s = 7.4$ as density parameter of the homogeneous electron gas, finding $\chi_P = 4.40 \times 10^{-6}$. This result neglects both electron-electron interactions and diamagnetic contribution χ_d of the electron gas itself. The electron-electron interaction is known to produce a strong enhancement factor $\lambda_{ee} = 2.35$, as estimated in Ref. [59]. For what concerns the diamagnetic contribution of the electron gas one can use the Landau diamagnetism estimate in the limit of effective electron mass equal to m , so that $\chi_d = -1/3\chi_P = -1.33 \times 10^{-6}$. The value of χ_P is rather low as compared to the experimental data of Fig. 7, while $\chi_{Li} = \chi_P \lambda_{ee} - \chi_P/3 = 8.89 \times 10^{-6}$, a value very close to the experimental value extrapolated to 20 MPM.

It is important to observe that, as the ammonia molecules maintain their structure almost unchanged [47] and their diamagnetic contribution was subtracted from the experimental data, the susceptibility reported in Fig. 7 is directly linked to the metallic regions around the lithium ions. As a consequence, the presence of a mild variation of the experimental χ_{Li} when $10 \leq \text{MPM} \leq 20$ is a signature of an almost concentration independent electron density of the metallic clusters. This signature is in good agreement with the electron gas esti-

mate at $r_s = 7.4$ and with the observed photoelectron spectra, and Ref. [52] with Ref. [47]. The agreement could be accidental, but c_∞ calculated using the same electron gas model is in agreement with the INS and IXS experiments. More important, the agreement in the case of paramagnetic susceptibility and collective mode velocity takes place when taking into account the important effect of the electron-electron interaction contribution [8,59], which is quite high due to the low electron density of the metallic regions. Therefore, when $\text{MPM} > 10$, both the paramagnetic susceptibility and the collective mode velocity c_∞ , as calculated including the effect of the electron-electron interaction [8,59], provide a convincing evidence of the presence of small metallic clusters having an almost fixed electron density, again in agreement with the observed photoelectron spectra of Ref. [47].

From the present analysis of the ion dynamics, using the neutron and x-ray data, where available, we first observe that the identification of a second mode allows for a simple description of the low frequency sound velocity c_0 as a function of Li concentration and temperature. The change of the mode-mode interaction parameter β_0 , necessary to describe the overall behavior of $S(Q, \omega)$, provides the correct trend of c_∞ and c_0 observed by direct determination [48]. The present results indicate that there is a change of the system properties at 10 MPM.

It is also found that at $Q \simeq 2 \text{ \AA}^{-1}$, that is a momentum close to the position of the major peak of $S(Q)$, the collective modes have a lower energy with a lower damping, a behavior characteristic of the de Gennes narrowing which can be a sort of reminiscence of the Brillouin zone periodicity in crystals. This effect is present in all samples so that it can be attributed to the ammonia cages the correlations of which contribute to the $S(Q)$ peak.

As to the damping it is seen that $\Gamma_1(Q)$ and $\Gamma_2(Q)$ have a more complex behavior than the almost linear one obtained using the single mode analysis of the previous studies and other liquid metals [8]. At very low Q there is the indication of a quadratic increase which looks like the hydrodynamic trend which, however, is lost very soon as Q grows and, as in other liquids, displays a less damped behavior. On increasing Q the damping shows some oscillation indicating that the sample at 10 MPM is different from those with higher Li content. Again, this is in agreement with the fact that around this Li concentration there is the general change observed in other experimental findings.

Finally we observe that the present combined data analysis witnesses the existence of a second mode having an optic-like dispersion relation at low Q . Indeed, a strong dip in both $\hbar\omega_{Q2}$ and $\hbar\Gamma_{Q2}$ is observed at $Q \approx 1 \text{ \AA}^{-1}$ (Fig. 6), though less evident at $\text{MPM} = 10$. At the same time, this is compatible with the behavior of the $j = 2$ mode intensity, showing not only a sharp maximum around 1.75 \AA , due to the overall static structure of the lithium-ammonia complexes, but also tells us that at shorter length scales we likely see the effect of other periodicities in time and space of the system. However, it is not easy to relate the observed behavior directly to the metallic nature of the system (varying with MPM), even if an evident difference is present at $\text{MPM} = 10$. As a consequence this point remains an open question and deserves further investigation.

ACKNOWLEDGMENTS

We acknowledge the ILL for providing neutron beam time. This research was funded by Ministero dell'Istruzione

dell'Università e della Ricerca Italiano (Grant No. PRIN2017-2017Z55KCW).

-
- [1] J. R. D. Copley and J. M. Rowe, Short-Wavelength Collective Excitations in Liquid Rubidium Observed by Coherent Neutron Scattering, *Phys. Rev. Lett.* **32**, 49 (1974).
- [2] N. H. March, *Liquid Metals* (Cambridge University Press, Cambridge, 1990).
- [3] E. Zurek, P. P. Edwards, and R. Hoffmann, A molecular perspective on lithium-ammonia solutions, *Angew. Chem. Int. Ed.* **48**, 8198 (2009).
- [4] C. Petrillo and F. Sacchetti, Future applications of the high-flux thermal neutron spectroscopy: The ever-green case of collective excitations in liquid metals, *Adv. Phys. X* **6**, 1871862 (2021).
- [5] V. M. Giordano and G. Monaco, Universal acoustic dispersion in liquid alkali metals, *Phys. Rev. B* **79**, 020201(R) (2009).
- [6] L. E. Bove, F. Sacchetti, C. Petrillo, and B. Dorner, Neutron Investigation of Collective Excitations in Liquid K-Cs Alloys: The Role of the Electron Density, *Phys. Rev. Lett.* **85**, 5352 (2000).
- [7] L. E. Bove, F. Sacchetti, C. Petrillo, and B. Dorner, Neutron Investigation of the Ion Dynamics in Liquid Mercury: Evidence for Collective Excitations, *Phys. Rev. Lett.* **87**, 215504 (2001).
- [8] L. Sani, C. Petrillo, and F. Sacchetti, Determination of the interstitial electron density in liquid metals: Basic quantity to calculate the ion collective-mode velocity and related properties, *Phys. Rev. B* **90**, 024207 (2014).
- [9] F. J. Bermejo, R. Fernandez-Perea, M. Alvarez, B. Roessli, H. E. Fischer, and J. Bossy, Collective, short-wavelength excitations in liquid gallium, *Phys. Rev. E* **56**, 3358 (1997).
- [10] T. Scopigno, A. Filippini, M. Krisch, G. Monaco, G. Ruocco, and F. Sette, High-Frequency Acoustic Modes in Liquid Gallium at the Melting Point, *Phys. Rev. Lett.* **89**, 255506 (2002).
- [11] L. E. Bove, F. Formisano, F. Sacchetti, C. Petrillo, A. Ivanov, B. Dorner, and F. Barocchi, Vibrational dynamics of liquid gallium at 320 and 970 K, *Phys. Rev. B* **71**, 014207 (2005).
- [12] C. A. Burns, P. M. Platzman, H. Sinn, A. Alatas, and E. E. Alp, Evidence for an Instability Near Twice the Fermi Wave Vector in the Low Electronic Density Liquid Metal $\text{Li}(\text{NH}_3)_4$, *Phys. Rev. Lett.* **86**, 2357 (2001).
- [13] A. H. Said, C. A. Burns, E. E. Alp, H. Sinn, and A. Alatas, Collective excitations in metal-ammonia systems as a function of electron density, *Phys. Rev. B* **68**, 104302 (2003).
- [14] F. Sacchetti, E. Guarini, C. Petrillo, L. E. Bove, B. Dorner, F. Demmel, and F. Barocchi, Giant electron-driven anomaly in the ion dynamics of a saturated solution of lithium in deuterated ammonia, *Phys. Rev. B* **67**, 014207 (2003).
- [15] P. Giura, R. Angelini, C. A. Burns, G. Monaco and F. Sette, Electron correlation effects on the dielectric function of liquid metals, [arXiv:cond-mat/0310336v2](https://arxiv.org/abs/cond-mat/0310336v2).
- [16] C. Petrillo, F. Sacchetti, E. Guarini, L. E. Bove, and F. Demmel, Collective modes in a saturated lithium-ammonia solution as a probe of the response of the low-density homogeneous electron gas, *Phys. Rev. B* **84**, 094206 (2011).
- [17] S. Hosokawa, M. Inui, Y. Kajihara, S. Tsutsui, and A. Q. R. Baron, Transverse excitations in liquid Fe, Cu and Zn, *J. Phys.: Condens. Matter* **27**, 194104 (2015).
- [18] M. Zanatta, F. Sacchetti, E. Guarini, A. Orecchini, A. Paciaroni, L. Sani, and C. Petrillo, Collective Ion Dynamics in Liquid Zinc: Evidence for Complex Dynamics in a Non-Free-Electron Liquid Metal, *Phys. Rev. Lett.* **114**, 187801 (2015).
- [19] B. G. del Rio and L. E. González, Longitudinal, transverse, and single-particle dynamics in liquid Zn: *Ab initio* study and theoretical analysis, *Phys. Rev. B* **95**, 224201 (2017).
- [20] S. Hosokawa, M. Inui, Y. Kajihara, S. Tsutsui, and A. Q. R. Baron, Transverse excitations in liquid Sn, *J. Phys.: Condens. Matter* **25**, 112101 (2013).
- [21] B. G. del Rio, M. Chen, L. E. González, and E. A. Carter, Orbital-free density functional theory simulation of collective dynamics coupling in liquid Sn, *J. Chem. Phys.* **149**, 094504 (2018).
- [22] E. Guarini, A. De Francesco, U. Bafle, A. Laloni, B. G. del Rio, D. J. González, L. E. González, F. Barocchi, and F. Formisano, Neutron Brillouin scattering and *ab initio* simulation study of the collective dynamics of liquid silver, *Phys. Rev. B* **102**, 054210 (2020).
- [23] F. Sette, G. Ruocco, M. Krisch, C. Masciovecchio, R. Verbeni, and U. Bergmann, Transition from Normal to Fast Sound in Liquid Water, *Phys. Rev. Lett.* **77**, 83 (1996).
- [24] C. Petrillo, F. Sacchetti, B. Dorner, and J.-B. Suck, High-resolution neutron scattering measurement of the dynamic structure factor of heavy water, *Phys. Rev. E* **62**, 3611 (2000).
- [25] F. Sacchetti, J.-B. Suck, C. Petrillo, and B. Dorner, Brillouin neutron scattering in heavy water: Evidence for two-mode collective dynamics, *Phys. Rev. E* **69**, 061203 (2004).
- [26] E. Pontecorvo, M. Krisch, A. Cunsolo, G. Monaco, A. Mermert, R. Verbeni, F. Sette, and G. Ruocco, High-frequency longitudinal and transverse dynamics in water, *Phys. Rev. E* **71**, 011501 (2005).
- [27] D. Bolmatov, M. Zhernenkov, D. Zav'yalov, S. Stoupin, A. Cunsolo, and Y. Q. Cai, Thermally triggered phononic gaps in liquids at THz scale, *Sci. Rep.* **6**, 19469 (2016).
- [28] M.-C. Bellissent-Funel, J. Teixeira, S.-H. Chen, B. Dorner, H. D. Middendorf, and H. L. Crespi, Low-frequency collective modes in dry and hydrated proteins, *Biophys. J.* **56**, 713 (1989).
- [29] D. Liu, X.-Q. Chu, M. Lagi, Y. Zhang, E. Fratini, P. Baglioni, A. Atlas, A. Said, E. Alp, and S.-H. Chen, Studies of Phononlike Low-Energy Excitations of Protein Molecules by Inelastic X-Ray Scattering, *Phys. Rev. Lett.* **101**, 135501 (2008).
- [30] A. Orecchini, A. Paciaroni, A. De Francesco, C. Petrillo, and F. Sacchetti, Collective dynamics of protein hydration water by Brillouin neutron spectroscopy, *J. Am. Chem. Soc.* **131**, 4664 (2009).
- [31] K. Yoshida, S. Hosokawa, A. Q. R. Baron, and T. J. Yamaguchi, Collective dynamics of hydrated β -lactoglobulin by inelastic x-ray scattering, *J. Chem. Phys.* **133**, 134501 (2010).
- [32] B. M. Leu, A. Alatas, H. Sinn, E. E. Alp, A. H. Said, H. Yavaş, J. Zhao, J. T. Sage, and W. J. Sturhahn, Protein elasticity probed

- with two synchrotron-based techniques, *J. Chem. Phys.* **132**, 085103 (2010).
- [33] A. Paciaroni, A. Orecchini, M. Haertlein, M. Moulin, V. Conti Nibali, A. De Francesco, C. Petrillo, and F. Sacchetti, Vibrational collective dynamics of dry proteins in the terahertz region, *J. Phys. Chem. B* **116**, 3861 (2012).
- [34] F. Sebastiani, A. Orecchini, A. Paciaroni, M. Jasnin, G. Zaccai, M. Moulin, M. Haertlein, A. De Francesco, C. Petrillo, and F. Sacchetti, Collective THz dynamics in living *Escherichia coli* cells, *Chem. Phys.* **424**, 84 (2013).
- [35] A. Paciaroni, A. Orecchini, G. E. Cornicchi, C. Petrillo, and F. Sacchetti, Glassy character of DNA hydration water, *J. Phys. Chem. B* **117**, 2026 (2013).
- [36] M. Zhernenkov, D. Bolmatov, D. Soloviov, K. Zhernenkov, B. P. Toperverg, A. Cunsolo, A. Bosak, and Y. Q. Cai, Revealing the mechanism of passive transport in lipid bilayers via phonon-mediated nanometre-scale density fluctuations, *Nat. Commun.* **7**, 11575 (2016).
- [37] G. D'Angelo, V. Conti Nibali, U. Wanderlingh, C. Branca, A. De Francesco, F. Sacchetti, C. Petrillo, and A. Paciaroni, Multiple interacting collective modes and phonon gap in phospholipid membranes, *J. Phys. Chem. Lett.* **9**, 4367 (2018).
- [38] D. Soloviov, Y. Q. Cai, D. Bolmatov, A. Suvorov, K. Zhernenkov, D. Zav'yalov, A. Bosak, H. Uchiyama, and M. Zhernenkov, Functional lipid pairs as building blocks of phase-separated membranes, *Proc. Natl. Acad. Sci. USA* **117**, 4749 (2020).
- [39] G. Jacucci and I. R. McDonald, Collective excitations in a liquid alloy, *J. Phys. F* **10**, L15 (1980).
- [40] A. Campa and E. G. D. Cohen, Observable Fast Kinetic Eigenmode in Binary Noble-Gas Mixtures? *Phys. Rev. Lett.* **61**, 853 (1988); Kinetic-sound propagation in dilute gas mixtures, *Phys. Rev. A* **39**, 4909 (1989).
- [41] N. Wisner and M. H. Cohen, Phase transitions of the electron fluid, *J. Phys. C: Solid State Phys.* **2**, 193 (1969).
- [42] B. K. Peters, K. X. Rodriguez, S. H. Reisberg, S. B. Beil, D. P. Hickey, Y. Kawamata, M. Collins, J. Starr, L. Chen, S. Udyavara, K. Klunder, T. J. Gorey, S. L. Anderson, M. Neurock, S. D. Minter, and Ph. S. Baran, Scalable and safe synthetic organic electroreduction inspired by Li-ion battery chemistry, *Science* **363**, 838 (2019).
- [43] N. Prasetyo, L. R. Canaval, K. Wijaya, and R. Armunanto, Lithium(I) in liquid ammonia: A quantum mechanical charge field (QMCF) molecular dynamics simulation study, *Chem. Phys. Lett.* **619**, 158 (2015).
- [44] V. V. Chaban, and O. V. Prezhdo, Electron solvation in liquid ammonia: Lithium, sodium, magnesium, and calcium as electron sources, *J. Phys. Chem. B* **120**, 2500 (2016).
- [45] B. Baranyi and L. Turi, Molecular dynamics simulations of solvated electrons in ammonia clusters, *J. Phys. Chem. B* **124**, 7205 (2020).
- [46] C. Fasolato, F. Sacchetti, P. Postorino, P. Tozzi, E. Principi, A. Simoncig, L. Foglia, R. Mincigrucci, F. Bencivenga, C. Masciovecchio, and C. Petrillo, Ultrafast Plasmon Dynamics in Crystalline LiF Triggered by Intense Extreme UV Pulses, *Phys. Rev. Lett.* **124**, 184801 (2020).
- [47] T. Buttersack, Ph. E. Mason, R. S. McMullen, H. C. Schewe, T. Martinek, K. Brezina, M. Crhan, A. Gomez, D. Hein, G. Wartner, R. Seidel, H. Ali, S. Thürmer, O. Marsalek, B. Winter, S. E. Bradforth, and P. Jungwirth, Photoelectron spectra of alkali metal-ammonia microjets: From blue electrolyte to bronze metal, *Science* **368**, 1086 (2020).
- [48] D. E. Bowen, J. C. Thompson, and W. E. Millett, Velocity of ultrasound in lithium-ammonia solutions, *Phys. Rev.* **168**, 114 (1968).
- [49] M. Inui, A. Koura, Y. Kajihara, S. Hosokawa, A. Chiba, K. Kimura, F. Shimajo, S. Tsutsui, and A. Q. R. Baron, Peculiar atomic dynamics in liquid GeTe with asymmetrical bonding: Observation by inelastic x-ray scattering, *Phys. Rev. B* **97**, 174203 (2018).
- [50] B. M. Powell, G. Dolling, G. S. Pawley, and J. W. Leech, Lattice-dynamics of ammonia, *Can. J. Phys.* **58**, 1703 (1980).
- [51] S. W. Lovesey, *Theory of Neutron Scattering from Condensed Matter* (Clarendon Press, Oxford, UK, 1984).
- [52] H. Thompson, J. C. Wasse, N. T. Skipper, S. Hayama, D. T. Bowron, and A. K. Soper, Structural studies of ammonia and metallic lithium-ammonia solutions, *J. Am. Chem. Soc.* **125**, 2572 (2003).
- [53] J. C. Wasse, S. Hayama, S. Masmanidis, S. L. Stebbings, and N. T. Skipper, The structure of lithium-ammonia and sodium-ammonia solutions by neutron diffraction, *J. Chem. Phys.* **118**, 7486 (2003).
- [54] <https://webbook.nist.gov/chemistry/>.
- [55] W.-C. Pilgrim, D. Szubrin, F. Demmel, A. Orecchini, S. Rols, A. Laloni and A. De Francesco, New perspectives onto the metal-to-non-metal transition in expanded liquid metals, *Europhys. Lett.* **122**, 36005 (2018).
- [56] X. Wang, C. A. Burns, A. H. Said, C. N. Kodituwakku, Y. V. Shvydko, D. Casa, T. Gog, and P. M. Platzman, Evolution of a strongly correlated liquid with electronic density, *Phys. Rev. B* **81**, 075104 (2010).
- [57] H. M. Böhm, S. Conti, and M. P. Tosi, Plasmon dispersion and dynamic exchange-correlation potentials from two-pair excitations in degenerate plasmas, *J. Phys.: Condens. Matter* **8**, 781 (1996).
- [58] A. Depriester, J. Fackeure, and J. P. Lelieur, Magnetic susceptibility of lithium-ammonia solutions, *J. Phys. Chem.* **85**, 272 (1981).
- [59] K. Utsumi and S. Ichimaru, Dielectric formulation of strongly coupled electron liquids at metallic densities. VII. Spin-dependent correlations, *Phys. Rev. B* **28**, 1792 (1983).